Reprogrammable Magnetically Actuated Self-Assembled (RMS) Cilia Array

Sukho Park[1]

[1]Affiliation not available

July 30, 2022

Sunwoo Sohn, Hyoryong Lee, Hyeonwoo Kee, Sukho Park*

Department of Robotics and Mechatronics Engineering, Daegu Gyeongbuk Institute of Science and Technology (DGIST), Daegu 42988, Republic of Korea

E-mail: *shpark12@dgist.ac.kr*

Keywords: reprogrammable artificial cilia; metachronal wave; biomimetics; magnetic actuators; fluidic channel

Abstract

Motile cilia move in an asymmetric pattern and implement a metachronal wave (MCW) to facilitate fluid movement in a viscous environment. Studies have been conducted to mimic MCW movement of motile cilia, but the fabrication process was too complicating or there were difficulties in accurately mimicking the shape of the cilia. To overcome these limitations, we introduce a self-assembly method to fabricate a reprogrammable magnetically actuated self-assembled (RMS) cilia array that can be reprogrammed by changing the magnetization direction through additional magnetization. Using the RMS cilia array, a unilateral cilia array (UCA) channel and a bilateral cilia array (BCA) channel were constructed, and the motion and fluid flow of the RMS cilia array were analyzed by applying different magnetic fields (strike magnetic field and rotating magnetic field). When a rotating magnetic field was applied to the UCA channel, a distinct MCW appeared. In the BCA channel test, fluid pumping was observed when a strike magnetic field, whereas fluid mixing was observed when a rotating magnetic field was applied. Based on these results, it is expected that the proposed RMS cilia array and magnetic field actuation method can be applied to lab-on-a-chip or microfluidic channels for fluid mixing and pumping.

1. Introduction

Cilia are hair-like, microtubule-based structures that have various distributions with a length of approximately 3–200 μm and an aspect ratio ranging from 10 to 100, depending on the location where they are found, and are divided into primary cilia and motile cilia.[1–5] Motile cilia can move objects or mix fluids by moving mucus or body fluids in the human body.[6,7] Among these motile cilia, the cilia that are found in the fallopian tube of the female reproductive system help the movement of the ovary, and the cilia existing in the lungs mix settled dust and bacteria through mucociliary clearance and move them out of the body.[8–10] The environment in which motile cilia move is normally filled with fluid with a low Reynolds number. In such an environment, the viscous force is generally more dominant than the inertial force, and has a significant influence on the fluid flow.[11–13] To be helpful in this environment, the cilium moves in an asymmetrical pattern comprising an effective stroke and a recovery stroke, creating a net fluid flow. In an effective stroke,

the cilium moves in an arc that is fully stretched, while in the recovery stroke, the cilium returns to the starting point in a bent state as if swinging, which increases the moving area of the cilium.[14–16] In addition, when several cilia gather to form a cilia array, they move in a sequential pattern that forms a wave called the metachronal wave (MCW), which helps move the fluid faster and more efficiently because of their asymmetrical motion.[17–20]

Several studies have reported mimicking the asymmetric motion of cilia and the MCW motion to efficiently pump or mix fluids in microfluidic devices with low Reynolds numbers.[21–23] To mimic cilia motion, many actuation methods have been used; actuation via a magnetic field is the most used method among them.[24–27] In addition, diverse manufacturing methods exist for magnetically actuated artificial cilia, and, the fabrication method using self-assembly has the advantages of simplicity and capability to mimic the appearance of natural cilia. However, it is difficult to program the magnetization direction, thus limiting the implementation of the MCW of the cilia.[28–31]

Nevertheless, studies have been conducted to imitate the metachronal wave of cilia by fabricating artificial cilia using the molding method, which facilitates reprogramming.[32,33] Nelson formed a cilia array using a molding method and then reprogrammed the cilia array, which moved the cilia array to form an MCW.[34] Sitti fabricated micro-cilia using a mold, magnetized each cilium independently, and attached them to form a cilia array with the desired arrangement that implements the MCW.[35] However, these studies actuated the cilia array using only a rotating external magnetic field, and because the cilia array was fabricated using the molding method, several complex steps were required for making the cilia array.

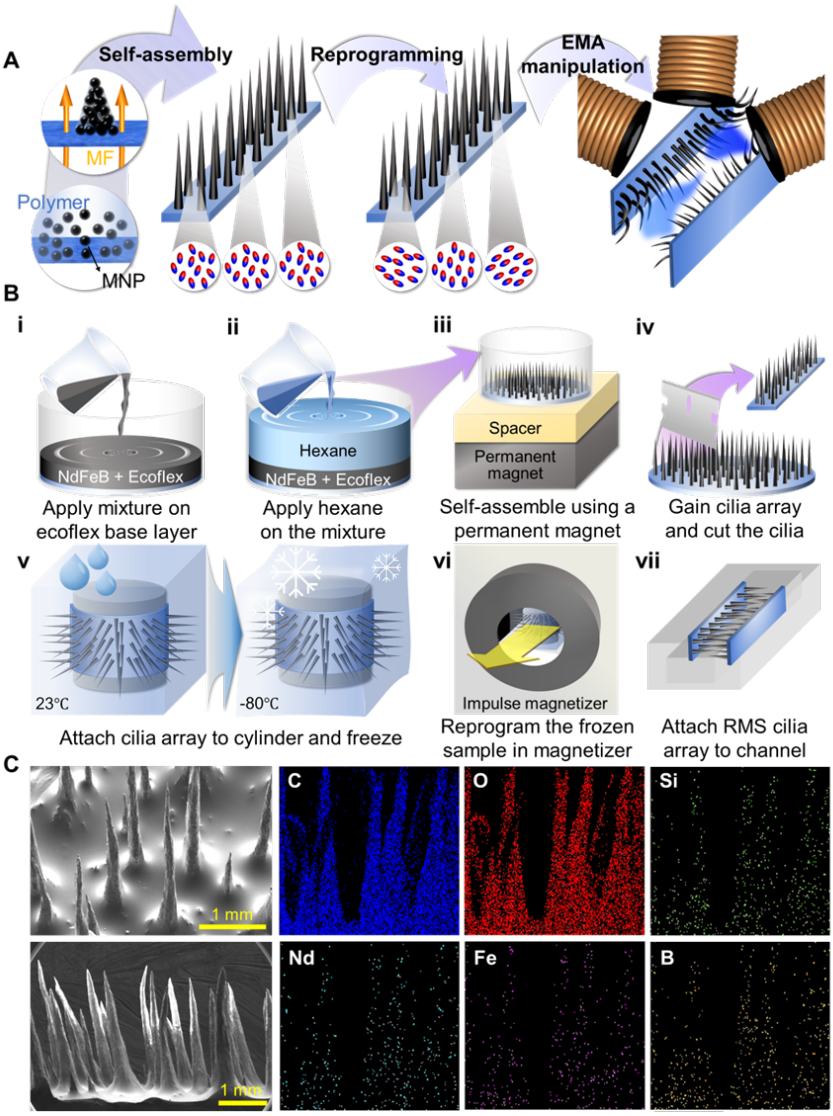

Figure 1 . (A) Concept of RMS cilia array; (B) Fabrication process of the RMS cilia array; Self-assembling process; (i) Add mixture of magnetic particles and silicone rubber on base layer, (ii) Add hexane to lower the silicone viscosity, (iii) Put the solution on the magnet to self-assemble the cilia, and (iv) Gain the final RMS cilia array and cut it into the required form; Reprogramming process; (v) Attach the RMS cilia array to a cylinder and freeze to hold place in the reprogramming process, (vi) Magnetize it in an impulse magnetizer to reprogram the magnetization direction of the cilia, and (vii) Channel fabrication process, and (C) SEM images and EDS analysis results of the RMS cilia

Moreover, the aspect ratio of the fabricated cilium is too small (approximately 5), which makes it difficult to mimic natural cilia with an aspect ratio of > 10.

To overcome the limitations of the reported artificial cilia array, we propose a reprogrammable magnetically actuated self-assembled (RMS) cilia array fabricated using a self-assembly method and reprogrammed by changing the magnetization direction of the cilia array as shown in Figure. 1A. Therefore, compared to the molding method used in previous studies, the cilia array can be easily developed and the shape and aspect

ratio of natural cilia can be mimicked using the proposed method. In addition, we implemented various motions of the RMS cilia array in fluids using an electromagnetic actuation (EMA) system that can form a magnetic field of the desired waveform.

2. Results

2.1. Fabrication of Reprogrammable Magnetically Actuated Self-Assembled Cilia Array

The RMS cilia array was fabricated using the self-assembly method, where NdFeB powder and Ecoflex 00-30 silicone rubber were mainly used for stretchability and magnetic manipulation (Figure. 1B). The fabricated RMS cilia have a shape similar to the actual cilia and show a length of approximately 3 mm, a bottom diameter of approximately 0.3 mm, and an aspect ratio of approximately 10 (Figure. 1C). EDS analysis was performed to confirm the components constituting the cilia (Figure. 1C). Consequently, it was confirmed that C, O, and Si elements constituting the Ecoflex silicone were detected at a high ratio, and Nd, Fe, and B elements were detected at a low ratio because the NdFeB particles were trapped inside the Ecoflex. To confirm the possibility of magnetic-field actuation, the magnetization value of the cilium was measured, and the saturation magnetization value of the cilium was approximately 68,608 A/m (**Figure. S1B**). In addition, the stress-strain graph was measured using a universal material testing machine, and Young's modulus (E) of the cilium was estimated to be approximately 211 kPa (Figure. S1C).

2.2. Fundamental Motions of RMS Cilia Arrays

Due to the ferromagnetic properties of the NdFeB particles, the RMS cilia array's magnetization direction can be reprogrammed using a magnetizer. In this experiment, the magnetization direction of the cilia array was selected, as shown in **Figure. 2A(i)** , from among the two magnetization directions for the RMS cilia array. To mimic the asymmetric motion of natural cilia, two types of magnetic fields (strike magnetic field and rotating magnetic field) were applied. When a strike magnetic field was applied to the cilium, an effective stroke due to the quick change of the magnetic field direction and a recovery stroke due to the slow return of the magnetic field direction to the original state could be implemented (Figure. 2B(i)). On the other hand, when a rotating magnetic field was applied, the cilium could follow the magnetic field and rotate along a plane to achieve an effective stroke and when the magnetic field could not overcome the elastic force of the cilium anymore, the cilium could snap back and rotate sideways to make a recovery stroke (Figure. 2B(ii)).

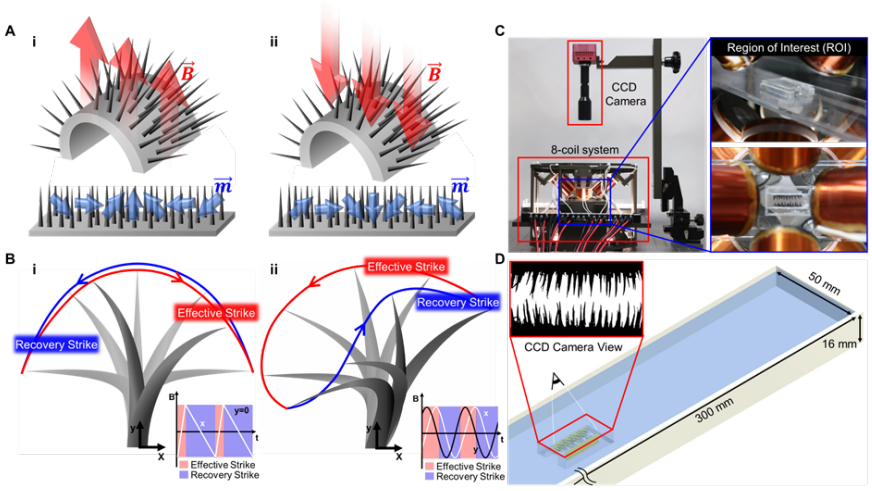

Figure 2. (A) Magnetization direction; (i) Cilia magnetized in the upper direction, (ii) Cilia magnetized

in the opposite direction, (B) Motion of a cilium manipulated by each field; (i) Strike magnetic field and (ii) Rotating magnetic field, (C) 8-coil electromagnetic system used actuation and CCD camera used for observation, and (D) Schematic of the acrylic channel and tank used in the experiment

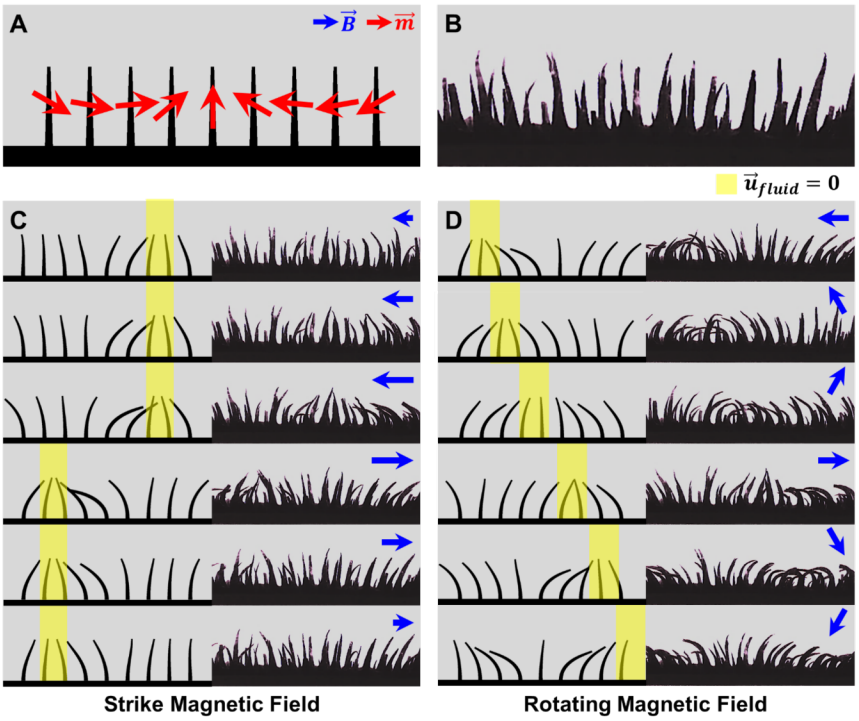

Figure 3. Comparison of the motion of cilia manipulated by the strike field and the rotating field in simulation and experiment, (A) Modeling of the RMS cilia array, (B) Actual RMS cilia array, (C) Motion of cilia when using the strike magnetic field, and (D) Motion of cilia when using the rotating magnetic field

When two different magnetic fields were applied, the experimental and FEM simulation results of the RMS cilia array were obtained (**Figure. 3** and **Movie S1**). First, the fabricated RMS cilia array was set (Figure. 3B) and simplified for the FEM analysis (Figure. 3A). Similar to the actual RMS cilia array, the simplified model used nine cilium models that were magnetized at angles of -120, -100, -90, -50, 0, 60, 90, 100, and 120 degrees. It was confirmed that the motions of the RMS cilia array by the strike magnetic field showed a very similar tendency in both the simulation and the experiment (Figure. 3C). The RMS cilia array, due to the strike magnetic field, did not show an MCW. However, through the movement of

the stagnation zone of the fluid flow, it was confirmed that the fluid flow could advance forward intermittently. Similarly, the motions of the RMS cilia array due to the rotating magnetic field in the experiment and simulation were very similar (Figure. 3D). In addition, when the rotating magnetic field was applied, the RMS cilia showed continuous motion, and through the sequential movement of the stagnation zone of the fluid flow, it was confirmed that the MCW was distinctly implemented, and the fluid flow could advance sequentially forward.

2.3. Fluid Tests using Unilateral Cilia Array Channel

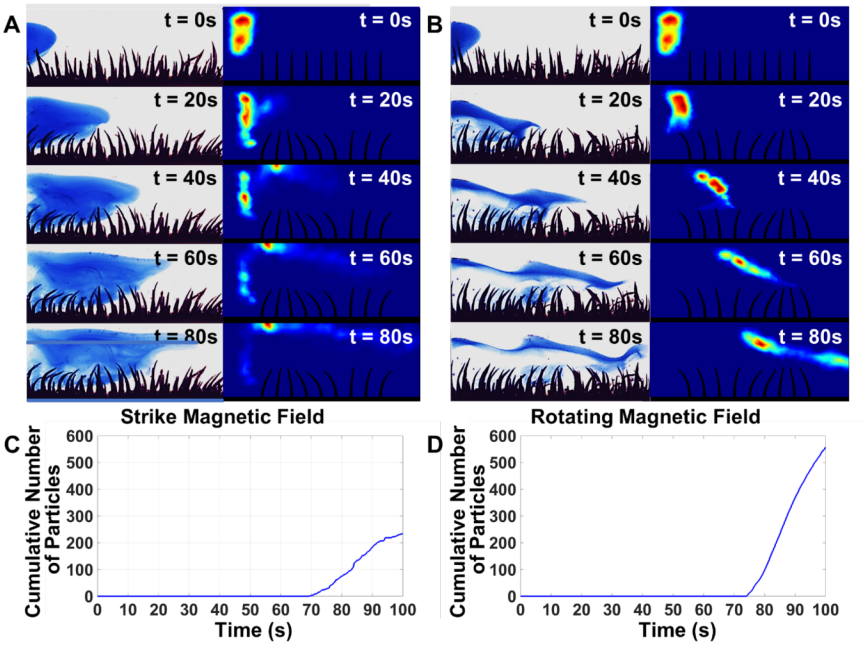

Figure 4. UCA channel test results, (A) Experimental and simulation results of particle movement due to the strike magnetic field, (B) Experimental and simulation result of particle movement due to the rotating magnetic field, (C) Cumulative number of particles that reached the outlet when the strike magnetic field was applied, and (D) Cumulative number of particles that reached the outlet when the rotating magnetic field was applied

A unilateral cilia array (UCA) channel was constructed and two types of magnetic fields (strike and rotating magnetic fields) were applied. We performed an experiment to confirm the difference in the fluid flow and a simulation to verify the experimental results (**Figure. 4** and **Movie S2**). When the strike magnetic field was applied to the UCA channel, the experimental results showed that the fluid flow, including particles, advanced very slowly, reaching approximately 15.75 mm in 80 s. Similar results were also confirmed through the simulation, such that the particles in the fluid moved forward slightly away from the UCA (Figure. 4A). In addition, it was confirmed through the graph showing the cumulative number of particles that the particles reached the channel outlet as time passed (Figure. 4C). When a rotating magnetic field was applied to the UCA channel, the experimental results confirmed that the fluid flow, including particles, moved forward following the tip of the UCA and reached the end of the channel by moving 18 mm in 80 s. The simulation results showed a similar tendency, in that the particles in the fluid moved rapidly along the tip of the UCA (Figure. 4B). In addition, all the particles reached the channel outlet after approximately 100 s (Figure. 4D).

Consequently, it was confirmed that the fluid flow containing particles moved forward in two types of magnetic fields in the UCA channel. When a rotating magnetic field was applied, the fluid moved faster than when a magnetic field was applied, and the particle movement pattern differed depending on the applied magnetic field. This is expected to be closely related to the distinct MCW that appeared when the rotating magnetic field was applied to the RMS cilia array shown in the fundamental motions.

2.4. Fluid Tests using Bilateral Cilia Array Channels

We constructed a Bilateral Cilia Array (BCA) channel by attaching two RMS cilia arrays to the top and bottom sides of the channel, based on the cilia array distributed within a narrow tube in the human body

(e.g., a fallopian tube). The BCA channel was composed of symmetric and asymmetric structures (**Figure. 5A**), and the optimal combinations for pumping and mixing, which are important functions of the cilia, were determined by applying strike and rotating magnetic fields via the EMA system and verifying through simulation.

To optimize each magnetic field, the tendency of fluid flow according to the frequency was observed. When the strike magnetic field is applied in both channels, the particle velocity increased with increasing frequency, peaking at 3 Hz and decreasing from 4 Hz (Figure. 5B). Furthermore, it was confirmed that particles were transmitted the fastest at 3 Hz through the coefficient of variation (CV), which quantifies the distribution of particles (**Figure. S2A, B**). When the rotating magnetic field was applied, the particle velocity increased as the frequency increased in both channels, continuously increasing up to 8 Hz and decreasing from 9 Hz (Figure. 5B). The CV values exhibited the same trend (Figure. S2C, D). In other words, the particles were most well dispersed at 8 Hz, and thus, the color intensity became uniform. Therefore, it was found that the performance was the best at 3 Hz for the strike magnetic field and 8 Hz for the rotating magnetic field.

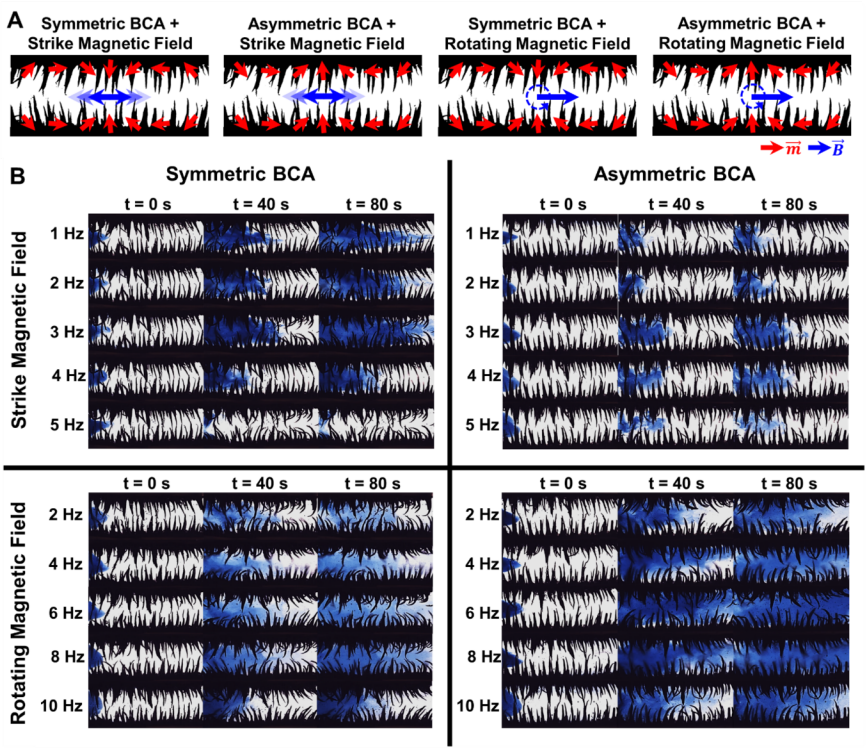

Figure 5. BCA channel frequency test results, (A) Magnetization direction of each BCA and intensity and direction or each magnetic field, and (B) Experiment result of fluid flow for 80 seconds for each BCA channel and each magnetic field

Based on the frequency with the best performance, fluid tests were conducted using configured BCA channels to confirm the tendency of fluid flow through the movement of the particles. When the strike magnetic field was applied, a strong pumping of the fluid flow appeared in the symmetric BCA channel (**Figure. 6A(i)** and **Movie S3**), where the average particle factor where the particles were located was 143 at t = 0 s and 195, with a standard deviation of 26.3 at t = 100 s, which implies that the fluid flow moved forward uniformly with little mixing. However, in the asymmetric BCA channel (Figure. 6A(ii) and **Movie S4**), most of the particles seemed to advance slowly up to 9 mm; however, after passing 9 mm, the particles

did not move well (Figure. 6B(ii)). When the rotating magnetic field was applied, the fluid was mixed by both the symmetric BCA channel and the asymmetric BCA channel (Figure. 6A(iii), (iv)); however, in the symmetric BCA channel, for 100 s, the particles were dispersed with a standard deviation of 26.3 (Figure. 6B(iii) and **Movie S5**). In the asymmetric BCA channel, the particles took approximately 60 s to spread evenly with a standard deviation of 9.9 (Figure. 6B(iv) and **Movie S6**). Consequently, the application of the strike magnetic field to the symmetric BCA channel was suitable for the pumping of the fluid because it maintained the particle concentration and advanced quickly, and the application of the rotating magnetic field to the asymmetric BCA channel was the fastest to make the particle distribution uniform, making it suitable for mixing.

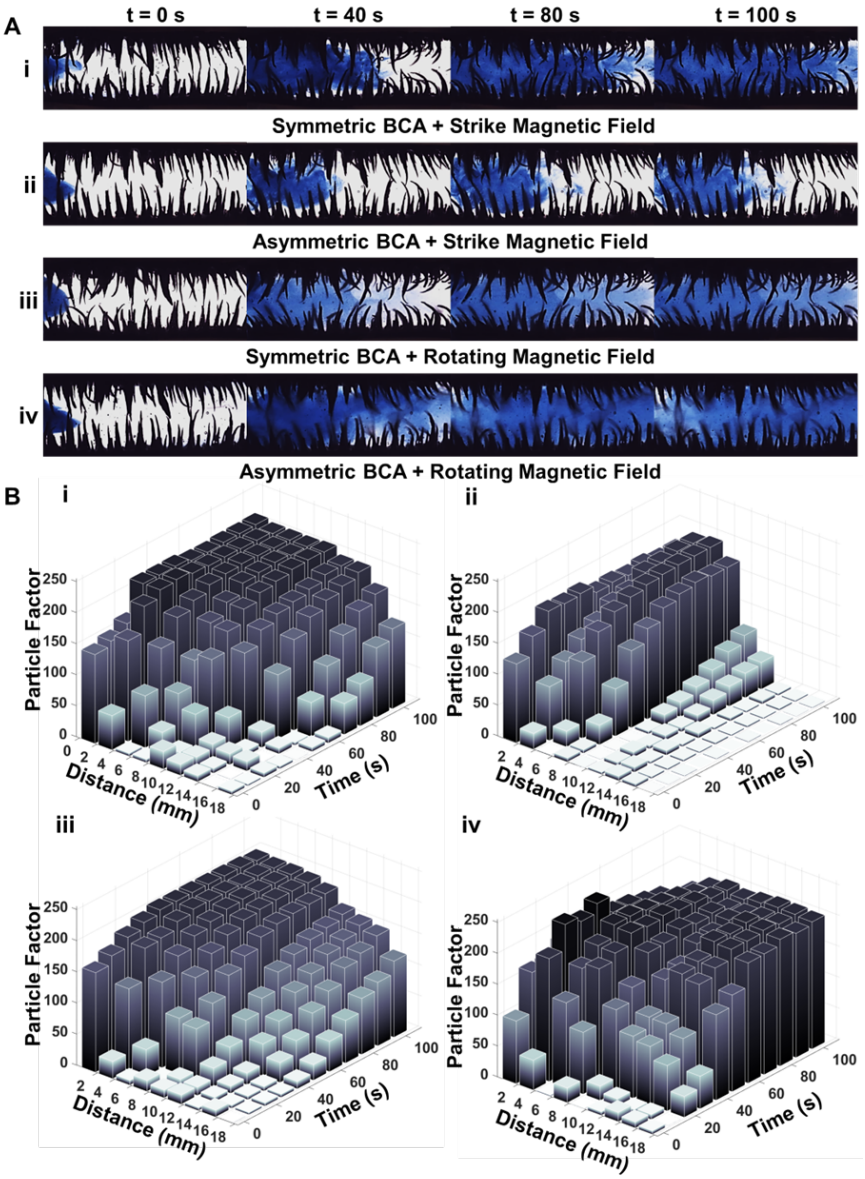

Figure 6 . BCA channel experiment results, (A) Experiment result of fluid flow for 100 seconds and (B) The variation of particle factor according to the position through time. The movement of the particles was

observed every 10 seconds; (i) Symmetric BCA + Strike Magnetic Field, (ii) Asymmetric BCA + Strike Magnetic Field, (iii) Symmetric BCA + Rotating Magnetic Field, and (iv) Asymmetric BCA + Rotating Magnetic Field

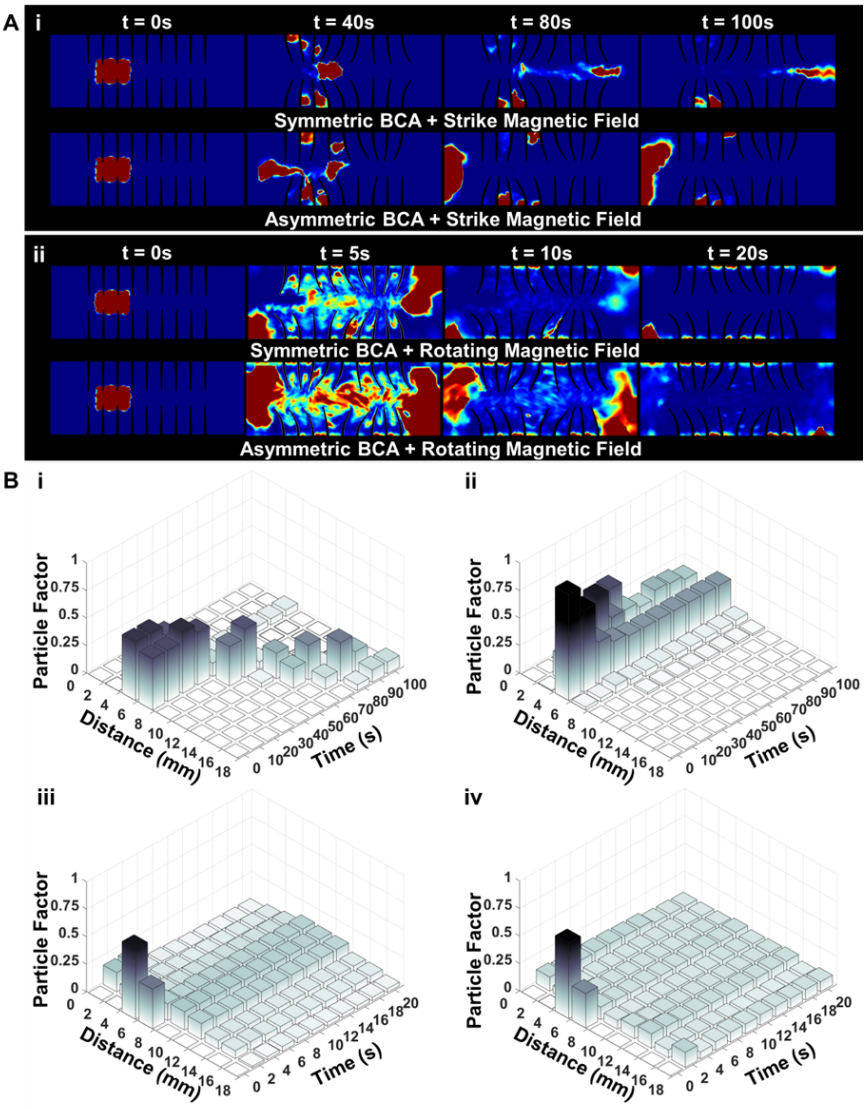

Figure 7. BCA channel simulation results, (A) Simulation result of particle density movement due to each cilia and field. The color scale shows the concentration of particles and (B) Relative number of particles counted according to the x-axis position throughout time; (i) Symmetric BCA + Strike Magnetic Field, (ii) Asymmetric BCA + Strike Magnetic Field, (iii) Symmetric BCA + Rotating Magnetic Field, and (iv) Asymmetric BCA + Rotating Magnetic Field

The particle distributions of the simulation confirmed that the motion of the fluid flow was largely divided according to the applied field type (strike and rotating field) (**Figure. 7** and **Movie S7**). When the strike magnetic field was applied, the fluid was pumped, which generally moved the particles forward. When the rotating magnetic field was applied, the fluid was mixed, which quickly dispersed the particles (Figure.

7A). This is similar to the experimental results (Figure. 6A), and could also be verified by the change in the number of particles (Figure. 7B). When the strike magnetic field was applied, in the symmetric BCA channel, the position where the particle number peaks had a strong property of moving forward rather than spreading (Figure. 7B(i)). In contrast, in the asymmetric BCA channel, the particles did not move forward but stayed in the middle (Figure. 7B(ii)). When the rotating magnetic field was applied, the particles were evenly dispersed throughout the symmetric BCA channel but did not spread well up to the inlet and outlet (Figure. 7B(iii)). However, it was found that the particles were evenly distributed up to the inlet and outlet throughout the asymmetric BCA channel (Figure. 7B(iv)). Through the simulations, it was also verified that when the strike magnetic field was applied, the symmetric BCA channel could show strong fluid pumping, and when the rotating magnetic field was applied, the asymmetric BCA could show distinct fluid mixing.

3. Discussion

The proposed RMS cilia array can be easily and conveniently fabricated using a self-assembly method, and the magnetization direction of the cilia can be reprogrammed. The fabricated cilia had a large aspect ratio (approximately 10), similar to the actual in vivo cilia, and could mimic the shape and movement of the actual cilia compared to previously reported studies. However, the size of the fabricated cilia (approximately 1–3 mm in length) is considerably larger than that of the actual cilia (approximately 4–10 μm in length). The size of the proposed cilia could be significantly affected by the particle size of the NdFeB powder, the external magnetic field, and the viscosity of the silicone. [36] Therefore, if NdFeB powder with small particle size, strong external magnetic field, and low silicon viscosity is used, it is expected that cilia with a smaller size can be fabricated. However, in this study, we attempted to mimic the shape and movement of real cilia through the RMS cilia array using the proposed self-assembly method and reprogramming.

The UCA channel was constructed using the RMS cilia array, and when two types of magnetic fields (strike and rotating magnetic fields) were applied to the channel, the asymmetric movement of the natural cilia could be mimicked and the generated fluid flow in the UCA channel was observed. When a rotating magnetic field is applied, MCW can be implemented; however, when a strike magnetic field is applied, MCW cannot be realized. However, in both types of magnetic fields, it was confirmed that the moving direction of the fluid changed sequentially, advancing the flow. When a magnetic field was applied, the fluid slowly moved forward as the fluid stagnation zone moved intermittently according to the movement of the cilia (Figure. 3C). However, when the rotating magnetic field was applied, the cilia moved to form an MCW, which moved the stagnation zone of the fluid sequentially (Figure. 3D). Therefore, the fluid in the UCA channel can advance faster under a rotating magnetic field.

In this study, symmetric and asymmetric BCA channels were constructed using the RMS cilia array, and when two types of magnetic fields (strike and rotating magnetic fields) were applied to each channel, the fluid flow was observed through experimentation and simulation. First, in the symmetric BCA channel, the upper and lower cilia arrays have the same magnetization direction along the x-axis and opposite magnetization directions along the y-axis. Therefore, when the strike magnetic field was applied, the upper and lower cilia arrays moved symmetrically, thereby creating a propelling fluid flow. On the other hand, when the rotating magnetic field was applied, the upper and lower cilia arrays showed propagation of the MCW in the same direction, but a phase difference occurred, which caused the rotating fluid flow rather than the propelling fluid flow. Additionally, in the asymmetric BCA channel, the upper and lower cilia arrays had opposite magnetization directions on both the x- and y-axes. Therefore, when the strike magnetic field was applied, the upper and lower cilia arrays moved in the opposite direction, which caused the fluid flow to return to the middle instead of advancing. In contrast, when the rotating magnetic field was applied, the upper and lower cilia arrays exhibited MCW propagation in opposite directions, resulting in a strong rotating fluid flow that caused the mixing of the fluid in the channel. As a result, when the strike magnetic field was applied to the symmetric BCA channel, the advancing fluid flow was generated owing to the symmetrical movement of the two cilia arrays, which is advantageous for fluid pumping. When a rotating magnetic field was applied to the asymmetric BCA channel, the propagation directions of the MCW of the upper and lower cilia arrays

were reversed, resulting in an asymmetrically rotating fluid flow, which is advantageous for fluid mixing.

All fluid experiments were conducted in a rectangular open channel with the inlet and outlet of 8 mm x 5 mm, and we used 70% glycerol diluted with distilled water which has a density of 1182.7 kg/m3 and a viscosity of 22.25 cp.[37] Herein, when the images of the UCA and BCA channel test results were analyzed, the flow velocity caused by the RMS cilia array has ranged from a minimum of about 0.2758 mm/s to a maximum of about 0.8328 mm/s. Based on the results, the Reynolds numbers in the experiments were calculated as the ranges from a minimum of 0.3222 to a maximum of 0.9728, which corresponds to the laminar flow section. Therefore, it is expected that repeatable results can be obtained when the experiment is executed under the above conditions.

In this study, to verify the experimental results, we conducted a simulation that showed trends very similar to those of the experiments. However, compared to the experimental results, the fluid flow for each magnetic field showed a similar trend, but there was a difference in the velocity of the fluid. This could be because of the limitations of the simulation. That is, a simplified model of the RMS cilia array was used in the simulation, but this model is not exactly equivalent and differs in terms of the pitch between the cilium, cilia length, and cilia thickness. In addition, the simulation was performed in a two-dimensional space, and because the cilia were recognized as a wall, the particles used could not pass through the cilia, and the fluid flow was significantly affected by the cilia structure. However, because the cilia array used in the experiment was arranged in a three-dimensional space, the particles in the fluid could pass through the space between cilia. In the future, for a more accurate simulation, it will be necessary to construct a precise simulation model with a shape similar to the cilia array used in the experiment and analyze the three-dimensional space of the simulation model.

4. Conclusion

In this study, the RMS cilia array was fabricated using a simple self-assembly method and had a shape and motion that was more similar to that of the natural cilia array than in previous studies. Using the RMS cilia array, a UCA channel was constructed, and by applying strike and rotating magnetic fields, the motion of the RMS cilia array and the resulting fluid flows were confirmed through experiments and simulations. Consequently, when the rotating magnetic field was applied, a clear MCW appeared, and the advancing movement of the particles in the fluid was also prominent. In addition, symmetric and asymmetric BCA channels were prepared and operated by applying strike and rotating magnetic fields, and the motion of the RMS cilia array in the BCA channels and the resulting fluid flows were confirmed through experiments and simulations. As a result, when the strike magnetic field was applied to the symmetric BCA channel, fluid pumping was observed, and when the rotating magnetic field was applied to the asymmetric BCA channel, fluid mixing was observed. Based on the above results, it is expected that the proposed RMS cilia array can be applied quickly and easily to lab-on-a-chip or microfluidic channels that require fluid mixing or pumping.

5. Experimental Section/Methods

Materials

NdFeB particles (MQFP-B-20076-089) from Magnequench (China), Ecoflex 00-30 from Smooth-On Inc. (USA), hexane (CH3(CH2)4CH3, extra pure) from Ducksan (South Korea), glycerol (HOCH2CH(OH)CH2OH, 99%) from Thermo Fisher, and blue fluorescent polystyrene particles from Bead & Micro (South Korea) were purchased and used.

Fabrication, Magnetization, and Characterization of Reprogrammable Magnetically Actuated Self-Assembled Cilia (RMS Cilia)

To fabricate the RMS cilia array, a mixture of NdFeB powder with an average size of 5 μm, EcoFlex 00-30 silicone rubber, and hexane at a 1:3:1 weight ratio was prepared using a planetary centrifugal mixer (ARM-310, THINKY). The NdFeB powder was used after being magnetized at 1.5 T in an impulse magnetizer

(IM-30, ASC Scientific) to improve its magnetization value. Then, an Ecoflex layer with a thickness of approximately 0.5 mm was made in a 35 mm [?] Petri dish, and 1 mL of the prepared mixture was poured on it (Figure. 1B(i)). Subsequently, 3 mL of hexane was added to the Petri dish, and the Petri dish was fixed at a distance of 30 mm using a spacer on a permanent magnet of 50 mm × 50 mm × 25 mm (Figure. 1B(ii), (iii)). After being placed in an oven at 60 °C for 2 h, the cilia array layer was separated from the Petri dish to obtain an RMS cilia array.

Second, to reprogram the magnetization direction of the fabricated RMS cilia array, the surface of the cilia array was treated with O_2 plasma (approximately 4 min) to make it hydrophilic, and the specimen was prepared by cutting it into a size of 20 mm × 5 mm (Figure. 1B(iv)). Then, using a 3D printer (DP200, Sindoh) to make a cylinder jig with a diameter of 9.5 mm and a height of 15 mm, the prepared cilia array layer specimen was wrapped on the cylinder jig, fixed with an instant adhesive, and placed in a 20 mm × 20 mm × 20 mm cube. To fix the posture of the cilia during the reprogramming process, the cubes were filled with water and placed in a deep freezer (-80 °C, 20 min) (Figure. 1B(v)). Subsequently, each cilium was magnetized to a magnitude of 1.5 T so that the magnetization angle was sequentially distributed from -120° to 120° (Figure. 1B(vi)). Finally, the frozen water in the cube was melted at room temperature, and the specimen was separated from the cylinder jig to obtain the final RMS cilia array.

Finally, the characteristics of the fabricated RMS cilia array were measured. First, shape imaging and EDS analysis of the fabricated cilia array were conducted using an ultra-high resolution FE-SEM (SU8230, Hitachi). The hysteresis loop of one cilium was measured using a vibration sample magnetometer (7404, Lake Shore Cryotonics), where the remnant flux density indicates the final magnetization value of the magnetized cilium. Finally, an experiment was performed to estimate the elastic modulus of cilia. A sample with the same weight composition (NdFeB:Ecoflex = 1:3) and a similar aspect ratio (10) with a diameter of 2 cm and a length of 20 cm was prepared, and the stress-strain graph of the prepared sample was measured using a universal testing machine (SFM-100kN, United Calibration). The elastic modulus of the cilium was estimated based on the measurements of the prepared sample.

Motion Measurement of RMS Cilia Array

An experiment was conducted to observe the motion of the RMS cilia array by using an external magnetic field. For this purpose, an acrylic channel with dimensions of 8 mm × 30 mm × 5 mm was used, an RMS cilia array was attached to the 30 mm × 5 mm side, and the 8 mm × 30 mm side was used for observation (Figure. 1B(vii)). The RMS cilia array was manipulated in the air using the magnetic field generated by an 8-coil EMA system (Figure. 2C). A magnetic field generated by the EMA system can be divided into a strike magnetic field in which the intensity of the magnetic field changes from -0.02 T to +0.02 T in the vertical direction of the cilia (Figure. 2B(i)) and a rotating magnetic field rotating from 0° to 360° with a constant intensity magnetic field of 0.02 T (Figure. 2B(ii)). When these two types of magnetic fields were applied, the motion of RMS cilia was observed using a CCD camera.

Flow Measurement in Fluid Channel using Unilateral and Bilateral RMS Cilia Array

In this study, to observe the fluid flow and particle behavior caused by the motion of the RMS cilia array, unilateral cilia array (UCA) and bilateral cilia array (BCA) channels were constructed, and the fluid flow was measured by applying two types of magnetic fields (strike and rotating magnetic fields). First, the same acrylic channel was used to measure the RMS cilia array motion, and both ends of the channel were opened (Figure. 1B(vii)). The channel was placed in the center of a 300 mm × 16 mm × 50 mm acrylic tank so that the channel was not affected by the tank wall as much as possible, and the channel was filled with 70 % glycerol solution (Figure. 2D).

First, in the UCA channel, a magnetized RMS cilia array was attached to one side of the channel and the channel was fixed in an acrylic tank. The 8-coil EMA system was used to apply the magnetic field for manipulation, and a CCD camera was used to observe the motion of the RMS cilia array and the resultant fluid flow. In particular, to observe the fluid flow, blue fluorescent polystyrene particles of size 5 μm were mixed with 70 % glycerol in a 1:4 volume ratio and 0.1 mL of this mixture was injected into the inlet of the

channel. Subsequently, two types of magnetic fields (strike and rotating magnetic fields) were applied, and the fluid flow was observed by conducting four experiments for 100 s.

Second, BCA channels (symmetric and asymmetric) were prepared using the two types of RMS cilia arrays (Figure. 2A). A symmetric BCA channel was fabricated, in which two RMS cilia arrays magnetized in the same direction were symmetrically attached to the channel. The asymmetric BCA channel was fabricated by attaching two RMS cilia arrays magnetized in opposite directions to the channel. The BCA channel experiment was performed using the same method as that for the previously described UCA channel. Additionally, we applied a strike magnetic field with a frequency of 1–5 Hz and a rotating magnetic field with a frequency of 1–10 Hz.

Particle Intensity Analysis for Fluid Flow Evaluation

In this study, to evaluate the tendency of fluid flow caused by the RMS cilia array in the channel experiments, an intensity analysis of the fluorescent particles in the fluid was performed using MATLAB. The images obtained from the channel experiments were analyzed at intervals of 20 s, and each image was divided into nine sections at intervals of 2 mm along the x-axis. The color intensity (0–255) values of the particles in each section were averaged using the following equation:

$$Average\_intensity\,(i) = Sum(i)/N(i) \quad \text{Equation 1}$$

where i is the number of sections, Sum $(i\ )$ represents the total color intensity in section i, and$N$ $(i\ )$ represents the number of pixels in section i , excluding cilia. As more particles were distributed in the section, darker images were obtained and lower intensity values were calculated. Therefore, the intensity value was inverted to describe the degree of particle distribution, and the inverted value was defined as the particle factor, given by the following equation.

$$Particle\_factor(i) = 255 - Average\_intensity(i) \quad \text{Equation 2}$$

Simulations of RMS Cilia Array

A finite element method (FEM) analysis was conducted using Multiphysics software (COMSOL, Inc., Stockholm, Sweden) to verify the experimental results confirming the motion of the RMS cilia array in the fluid by an external magnetic field, the fluid flow generated by the motion, and the particle movement caused by the generated fluid flow. The FEM analysis was performed using the following process.

First, the AC/DC module was used for FEM analysis of the torque received by the RMS cilia array from the external magnetic field. In this study, a magnetic field of 0.02 T was applied to manipulate the cilium, which has a magnetization value of 68,608 A/m. Based on these values, the magnetic flux density in the cilium was calculated, and the force applied to the cilium was calculated using the Maxwell stress tensor.

Second, the fluid-structure interaction (FSI) module was used for the FEM analysis of cilia motion by an external magnetic field and the fluid flow generated by cilia motion. The modeled cilium was set as a nearly incompressible linear elastic material, and the force applied to the cilium was applied as the boundary load of the cilium in this module. At this time, the fluid flow in the channel according to the motion of the cilia was analyzed using incompressible Navier-Stokes equations for the velocity and pressure fields, and the channel wall was set as a no-slip condition.

Finally, the particle-tracing module was used to verify the motion tendency of the particles by the fluid flow generated by the RMS cilia array. The motion equation for each particle was calculated using Newton's second law, considering the force applied to the particle by the fluid flow and drag force of the particle in the fluid.

Acknowledgments

This work was supported by the National Research Foundation (NRF), funded by the Ministry of Science and ICT (NRF-2021R1A2C3007817), and the Korea Health Industry Development Institute (KHIDI) funded

by the Ministry of Health & Welfare (HI19C0642), Republic of Korea.

References

1. J.R. Broekhuis, W.Y. Leong, G. Jansen, *Int. Rev. Cell. Mol. Biol.* **2013** , 303, 101–138.
2. P. Satir, S.T. Christensen, *Annu. Rev. Physiol.* **2007** , 69, 377–400.
3. D.M. Supp, D.P. Witte, S.S. Potter, M. Brueckner, *Nature* .**1997** , 389, 963–966.
4. W.A. Abou Alaiwi, S.T. Lo, S.M. Nauli, *Sensors* . **209** , 9, 7003–7020.
5. D.N. Wheatley, *Pathobiol.* **1995** , 63, 222–238.
6. J.C. Nawroth, H. Guo, E. Koch, E.A.C. Heath-Heckman, J.C. Hermanson, E.G. Ruby, J.O. Dabiri, E. Kanso, M. McFall-Ngai, *Proc. Natl. Acad. Sci. U.S.A.* **2017** , 114, 9510–9516.
7. Y. Ding, J.C. Nawroth, M.J. McFall-Ngai, E. Kanso, *J. Fluid Mech.* **2014** , 743, 124–140.
8. A.S. Shah, Y. Ben-Shahar, T.O. Moninger, J.N. Kline, M.J. Welsh,*Science.* **2009** , 325, 1131–1134.
9. R.A. Lyons, E. Saridogan, O. Djahanbakhch, *Hum. Reprod. Update.***2006** , 12, 363–372.
10. S. Chateau, U. d'Ortona, S. Poncet, *J. Favier, Front. Physiol.***2018** , 9, 161.
11. E.M. Purcell, *Am. J. Phys.* **1977** , 45, 3–11.
12. M.A. Sleigh, J.R. Blake, N. Liron, *Am. Rev. Respir. Dis.***1988** , 137, 726–741.
13. C. Brennen, H. Winet, *Annu. Rev. Fluid Mech.* **1977** , 9, 339–398.
14. S.A. Baba, *Nature.* **1979** , 282, 717–720.
15. P. Satir, *Sci. Am.* **1974** , 231, 44–54.
16. C. Barton, S. Raynor, *Bull. Math. Biophys.* **1967** , 29, 419–428.
17. E. Aiello, M.A. Sleigh, *J. Cell. Biol.* **1972** , 54, 493–506.
18. S. Gueron, K. Levit-Gurevich, N. Liron, J.J. Blum, *Proc. Natl. Acad. Sci. U.S.A.* **1997** , 94, 6001–6006.
19. J. Elgeti, G. Gompper, *Proc. Natl. Acad. Sci. U.S.A.***2013** , 110, 4470–4475.
20. P. Satir, *J. Cell. Biol.* **1963** , 18 345–365.
21. E. Milana, B. Gorissen, S. Peerlinck, M. de Volder, D. Reynaerts,*Adv. Funct. Mater.* **2019** , 29, 1900462.
22. S. Hanasoge, M. Ballard, P.J. Hesketh, A. Alexeev, *Lab. Chip.***2017** , 17, 3138–3145.
23. S.N. Khaderi, J.M.J. den Toonder, P.R. Onck, *J. Fluid. Mech.***2011** , 688, 44–65.
24. J. den Toonder, F. Bos, D. Broer, L. Filippini, M. Gillies, J. de Goede, T. Mol, M. Reijme, W. Talen, H. Wilderbeek, *Lab. Chip.***2008** , 8, 533–541.
25. F. Fahrni, M.W.J. Prins, L.J. van IJzendoorn, *Lab. Chip.***2009** , 9, 3413–3421.
26. S. Sareh, J. Rossiter, A. Conn, K. Drescher, R.E. Goldstein, *J. R. Soc. Interface.* **2013** , 10, 20120666.
27. S.N. Khaderi, C.B. Craus, J. Hussong, N. Schorr, J. Belardi, J. Westerweel, O. Prucker, J. Rühe, J.M.J. den Toonder, P.R. Onck,*Lab. Chip.* **2011** , 11, 2002–2010.
28. X. Zhang, J. Guo, X. Fu, D. Zhang, Y. Zhao, *Adv. Intell. Syst.***2021** , 3, 2000225.
29. S. Hanasoge, P.J. Hesketh, A. Alexeev, *ACS Appl. Mater. Interfaces.* **2020** , 12, 46963–46971.
30. Y. Wang, Y. Gao, H. Wyss, P. Anderson, J. den Toonder, *Lab. Chip.* **2013** , 13, 3360–3366.
31. M. Vilfan, A. Potočnik, B. Kavčič, N. Osterman, I. Poberaj, A. Vilfan, D. Babič, *Proc. Natl. Acad. Sci. U.S.A.* **2010** , 107, 1844–1847.
32. R. Marume, F. Tsumori, K. Kudo, T. Osada, K. Shinagawa, *Jpn. J. Appl. Phys.* **2017** , 56, 06GN15.
33. S. Zhang, R. Zhang, Y. Wang, P.R. Onck, J.M.J. den Toonder, *ACS Nano.* **2020** , 14, 10313–10323.
34. H. Gu, Q. Boehler, H. Cui, E. Secchi, G. Savorana, C. de Marco, S. Gervasoni, Q. Peyron, T.-Y. Huang, S. Pane, *Nat. Commun.***2020** , 11, 1–10.
35. X. Dong, G.Z. Lum, W. Hu, R. Zhang, Z. Ren, P.R. Onck, M. Sitti,*Sci. Adv.* **2020** , 6, eabc9323.
36. J.V.I. Timonen, C. Johans, K. Kontturi, A. Walther, O. Ikkala, R.H.A. Ras, *ACS Appl. Mater. Interfaces.* **2010** , 2, 2226–2230.
37. J. B., Segur, H. E. Oberstar, *Ind. Eng. Chem.* **1951** , 43, 2117-2120.

Table of Contents

A reprogrammable magnetically actuated self-assembled (RMS) cilia array which has a shape and motion similar to natural cilia is proposed. It shows asymmetric motion and MCW by reprogramming and applying strike and rotating magnetic fields. Particle movements are examined in fluid tests and analyzed through simulations to confirm the best channel and magnetic field combination for fluid pumping/mixing.

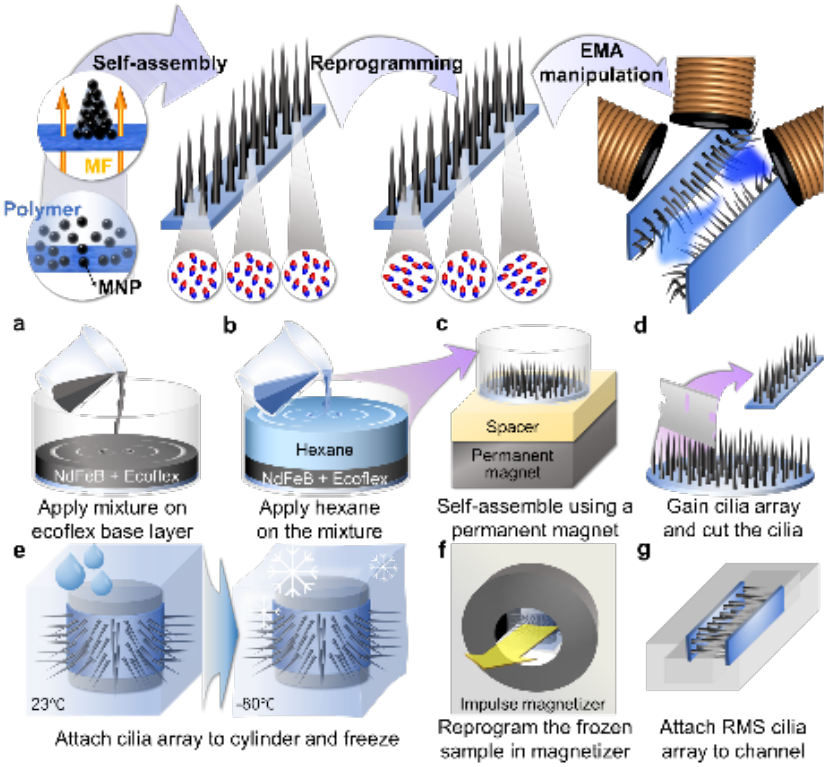

Supporting Information

In this paper, a reprogrammable magnetically actuated self-assembled (RMS) cilia array was fabricated which has a simple fabrication process and whose magnetization direction can be modified. To analyze the characteristics of the RMS cilia, samples were prepared, and magnetization and young's modulus were measured using VSM and the universal testing machine, respectively. First, to measure VSM, one cilium was cut out from the RMS cilia array and used as a measurement specimen. In the case of the universal testing machine, the cilium did not match the testing scale, so the sample was prepared with NdFeB powder, EcoFlex, and hexane in a 1:3:1 weight ratio, which is the ratio used to fabricate the RMS cilia. The results measured using each sample is shown in Figure S1. The magnetization of a cilium was 68,608 A/m and the Young's modulus (E) of cilium was about 211 kPa.

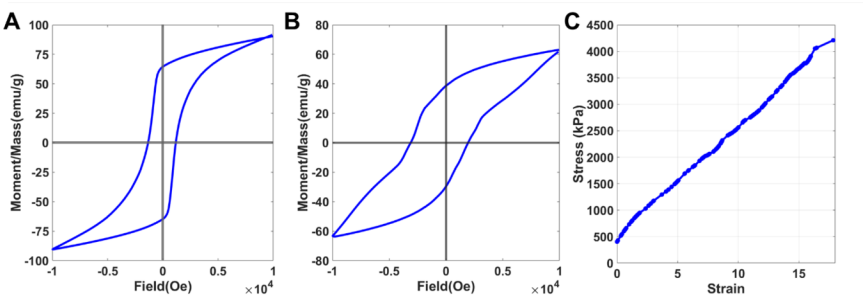

Figure S1 . Characteristics of fabricated RMS cilia array: VSM result of (A) NdFeB powder and (B) a cilium and (B) Stress-strain curve of NdFeB + Ecoflex sample.

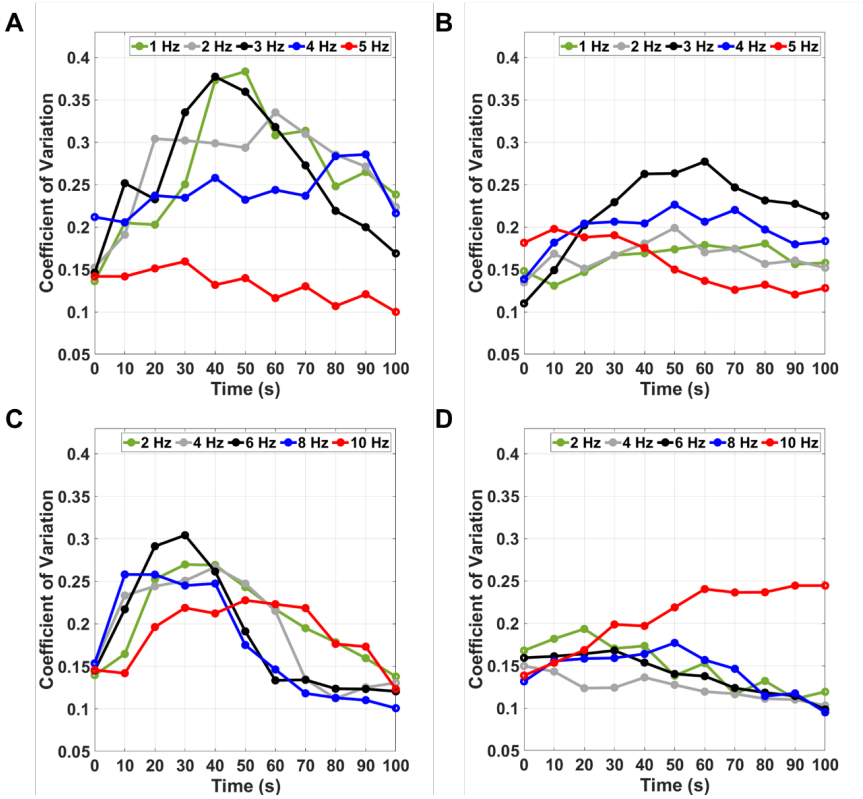

Figure S2 . Analysis of particle distribution of the BCA channel test results using the coefficient of variables (CV): (A) Symmetric BCA + Strike Magnetic Field, (B) Asymmetric BCA + Strike Magnetic Field, (C) Symmetric BCA + Rotating Magnetic Field and (D) Asymmetric BCA + Rotating Magnetic Field.

A BCA channel was fabricated with the RMS cilia and using it, fluid tests were performed. The experimental results according to the type of each channel and each magnetic field were evaluated by analyzing the particle distribution and the traveled distance of the particles. In the case of particle distribution, the image was analyzed using the coefficient of variation (CV), which is a value the standard deviation of the color intensity of the image divided by the mean value of the color intensity of the image. In this case, the lower the CV value, the better the particle distribution is. First, it can be seen that the CV value increases and decreases from 1 to 4 Hz when a strike magnetic field is applied which is shown in Figure S2A and Figure S2B. It can be seen that the particles move forward and then converge to the same concentration as a whole.

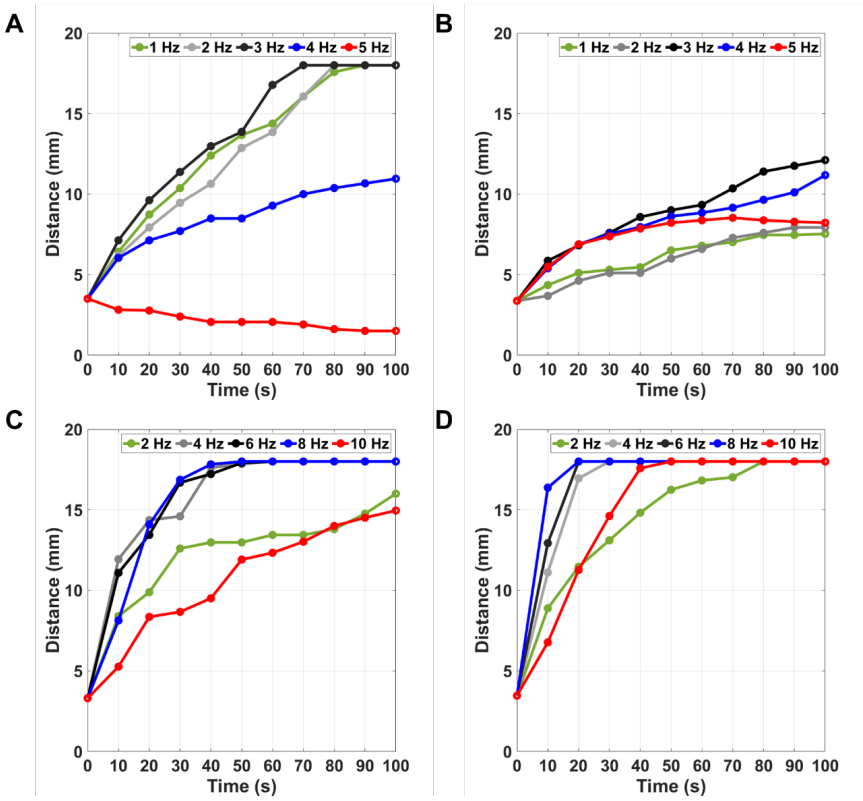

Figure S3 . Analysis of particle distance of the BCA channel test results: (A) Symmetric BCA + Strike Magnetic Field, (B) Asymmetric BCA + Strike Magnetic Field, (C) Symmetric BCA + Rotating Magnetic Field and (D) Asymmetric BCA + Rotating Magnetic Field.

In particular, it can be seen that the particles are most rapidly distributed at 3 Hz, and then decreases after. Also, in the case of symmetric BCA at 100 seconds, it can be seen that the CV value is lower than that of asymmetric BCA, confirming that the particles have moved as a whole. When a rotating magnetic field is applied, it can be seen that the distribution of the particles increases as the frequency increases up to 8 Hz and decreases thereafter as shown in Figure S2C and Figure S2D. Both symmetric BCA and asymmetric BCA have the best performance at 8 Hz, and it can be seen that asymmetric BCA converges quickly among the two, resulting in faster distribution.

Figure S3 shows the distance traveled by the particles, which was analyzed based on the maximum x-axis distance reached by receiving the particle position by analyzing color intensity. When a strike magnetic field is applied, it can be seen that in Figure S3A, when using the symmetric BCA, the particles reach the end of the channel, 18mm, but not in the case of asymmetric BCA shown in Figure S3B. Also, it shows that the particles move the fastest at 3 Hz and then the speed decreases. When a rotating magnetic field is applied, the particles reach the end of the channel faster than when a strike magnetic field is applied. In detail, it can be seen that the particles move faster in the asymmetric BCA than in the symmetric BCA. Also, the performance is the best at 8 Hz, and the traveled distance of the particles decreases thereafter.

Hosted file

`Movie S1- Fundamental Motions of RMS Cilia Array-mp4.mov` available at https://authorea.com/

users/441864/articles/578907-reprogrammable-magnetically-actuated-self-assembled-rms-cilia-array

Hosted file

Movie S2- Unilateral Cilia Array Channel Test Results-mp4.mov available at https://authorea.com/users/441864/articles/578907-reprogrammable-magnetically-actuated-self-assembled-rms-cilia-array

Hosted file

Movie S3- Bilateral Cilia Array Channel Test Results (Symmetric BCA + Strike Magnetic Field)-mp4.mov available at https://authorea.com/users/441864/articles/578907-reprogrammable-magnetically-actuated-self-assembled-rms-cilia-array

Hosted file

Movie S4- Bilateral Cilia Array Channel Test Results (Asymmetric BCA + Strike Magnetic Field)-mp4.mov available at https://authorea.com/users/441864/articles/578907-reprogrammable-magnetically-actuated-self-assembled-rms-cilia-array

Hosted file

Movie S5- Bilateral Cilia Array Channel Test Results (Symmetric BCA + Rotating Magnetic Field)-mp4.mov available at https://authorea.com/users/441864/articles/578907-reprogrammable-magnetically-actuated-self-assembled-rms-cilia-array

Hosted file

Movie S6- Bilateral Cilia Array Channel Test Results (Asymmetric BCA + Rotating Magnetic Field).mov available at https://authorea.com/users/441864/articles/578907-reprogrammable-magnetically-actuated-self-assembled-rms-cilia-array

Hosted file

Movie S7- Bilateral Cilia Array Simulation Results.mov available at https://authorea.com/users/441864/articles/578907-reprogrammable-magnetically-actuated-self-assembled-rms-cilia-array